

Supporting Information

Tuning the porosity and photocatalytic performance of triazine-based graphdiyne polymers *via* polymorphism

Dana Schwarz, Amitava Acharjya, Arun Ichangi, Yaroslav S. Kochergin, Pengbo Lyu, Maksym V. Opanasenko, Ján Tarábek, Jana Vacek Chocholoušová, Jaroslav Vacek, Johannes Schmidt, Jiří Čejka, Petr Nachtigall, Arne Thomas and Michael J. Bojdys*

DOI: 10.1002/anie.2016XXXXX

Table of Contents

Experimental Procedures	3
Materials.....	3
Methods	3
Synthesis.....	5
Fourier-transform infrared (FT-IR) spectroscopy	7
Thermogravimetric analysis (TGA)	8
X-ray photoelectron spectroscopy (XPS).....	9
Energy dispersive X-ray (EDX) spectroscopy	10
Powder X-ray diffraction (PXRD).....	12
Transmission electron microscopy (TEM).....	13
Scanning electron microscopy (SEM).....	13
Theoretical calculations	14
Argon (Ar) sorption and pore analysis	17
Carbon dioxide (CO ₂) sorption.....	17
Porosity parameters	18
Photocatalysis	18
Author Contributions.....	18
References	19

SUPPORTING INFORMATION

Experimental Procedures

Materials

All chemicals and solvents were used as received without any further purification steps before using them. All reactions were carried out under an argon atmosphere in flame-dried glassware on a Schlenkline. Completion of reactions was determined by TLC using silica gel (Merck 60, F-254) covered aluminum plates and visualized by UV detection ($\lambda = 254$ nm). Purification by column chromatography was performed using silica gel (0.063 – 0.2 mm, 100 mesh ASTM) from Penta s.r.o. All solvents used for the reaction were purchased from VWR and were anhydrous except for pyridine. 4-bromobenzonitrile, trifluoromethanesulfonic acid (TFMSA) were purchased from Acros Organics. Pd(PPh₃)₄ and 1.6 M *n*-butyllithium in hexane were purchased from Sigma Aldrich. Anhydrous ZnCl₂ was purchased from Alfa-Aesar. Ethenyltrimethylsilane was purchased from ABCR.

Methods

¹H and ¹³C NMR spectra of the monomers in CDCl₃ as well as **solid-state cross-polarisation magnetic-angle spinning (CP-MAS)** spectra were recorded on a Bruker Advance 400 instrument. Chemical shifts (δ) were reported in ppm (internal standard CHCl₃ for liquid measurements was set at $\delta_{\text{H}} = 7.26$ ppm). ¹³C CP-MAS NMR experiments were carried out at a MAS rate of 12.0 kHz using zirconia rotors 4 mm in diameter. The spectrum was measured using a contact time of 10 ms and a relaxation delay of 10.0 s.

Fourier-transform infrared (FT-IR) spectra were recorded from KBr pellets on an AVATAR 370 FT-IR spectrometer from Thermo Nicolet.

Inductively coupled plasma optical emission spectrometry (ICP-OES) measurements were performed using the SPECTRO ARCOS optical emission spectrometer (SPECTRO Analytical Instruments, Kleve, Germany) with radial plasma observation. The SPECTRO ARCOS features a Paschen-Runge spectrometer mount; the wavelength range between 130 and 770 nm can be simultaneously analysed. An air-cooled ICP-generator is installed based on a free-running 27.12 MHz system. For sample introduction, a cyclonic spray chamber and a modified Lichte nebuliser were used. The following ICP operating parameters were applied: generator power 1 450 W, coolant flow 13 L/min, auxiliary flow 0.8 L/min, nebuliser flow 0.75 L/min, sample aspiration rate 2 mL/min. For calibration, commercially available multi-element standard solutions (Analytika, Czech republic) were used. The concentrations of calibrated elements were 0, 0.2, 1.0, 5.0, 10.0 and 20.0 mg/L, respectively. 2 mg/L Y was used as an internal standard. All measurements were performed in 4% HNO₃ as a matrix. Sample preparation: the solid samples were weighted (approx. 5 mg) on microanalytical balance and combusted by the Schöniger method. After combustion, the closed Erlenmeyer flask was treated in an ultrasonic bath for several minutes. After absorption of combustion products (for at least 2 h) 50 μ l of 1000 mg/L of Y standard solution was added (final concentration 2 mg/L). Afterwards, the liquid mixture was transferred from the glass flask into a plastic bottle. The flask was rinsed carefully with deionised water. The concentration of HNO₃ was adjusted to 4% (w/w in final volume). Then deionised water was added to achieve the final volume of 25 mL. After mixing, the solution was filtered and introduced to the spectrometer system.

Thermogravimetric analysis (TGA) was performed on a Setsys Evolution 18 with temperature range up to 1750 °C. All samples were measured in alumina crucibles. The heating rate was 5 K min⁻¹.

X-ray photoelectron spectroscopy (XPS) was performed with an AXIS ULTRA (Kratos Analytical, England). For the measurement a Mono-Al K $\alpha_{1,2}$ X-ray-source was used with a rated input of the x-ray tube of 300 W at 20 mA. The analyser had a pass energy of 160 eV (overview spectra), and 20 eV (high resolution spectra), respectively. For charge compensation, a low energy electron source (Filament) in contact with a magnetic immersion lens was used.

Energy dispersive X-ray (EDX) spectroscopy was performed using the energy-dispersive X-ray analyzer INCA 250 on the Nova NanoSEM 450, FEI. EDX spectra were obtained at a working voltage of 20 kV.

Powder X-ray (XRD) data was obtained on a Bruker D8 Advance using Cu K α_1 radiation with secondary graphite monochromator and LYNXEYE XE detector.

Transmission electron microscopy (TEM) and the corresponding selected area electron diffraction (SAED) were performed on JEOL JEM-2200FS field emission electron microscope, operating at an accelerating voltage of 200 kV. The specimens for HR-TEM imaging were prepared by sonication of the samples in anhydrous iso-propanol (IPA); the dispersion was then drop-coated onto a copper grid with carbon support film and dried on a heating stage.

Scanning electron microscope (SEM) images were obtained on a Nova NanoSEM 450 from FEI.

Solid-state Raman spectra were recorded on a DXR Raman spectrometer (Thermo Scientific) interfaced to an Olympus microscope, employing an objective 10x using the 532 nm (diode-pumped solid-state laser) excitation lines. The laser power ranged from 2 to 10 mW. The full-scale grating was used for all measurements.

SUPPORTING INFORMATION

Solid-state UV/Vis measurements were taken on a UV-2550 from Shimadzu.

Photoluminescence (PL) spectra were measured with a Fluorolog-3 FL3-22 spectrofluorometer (Horiba – Jobin Yvon, France).

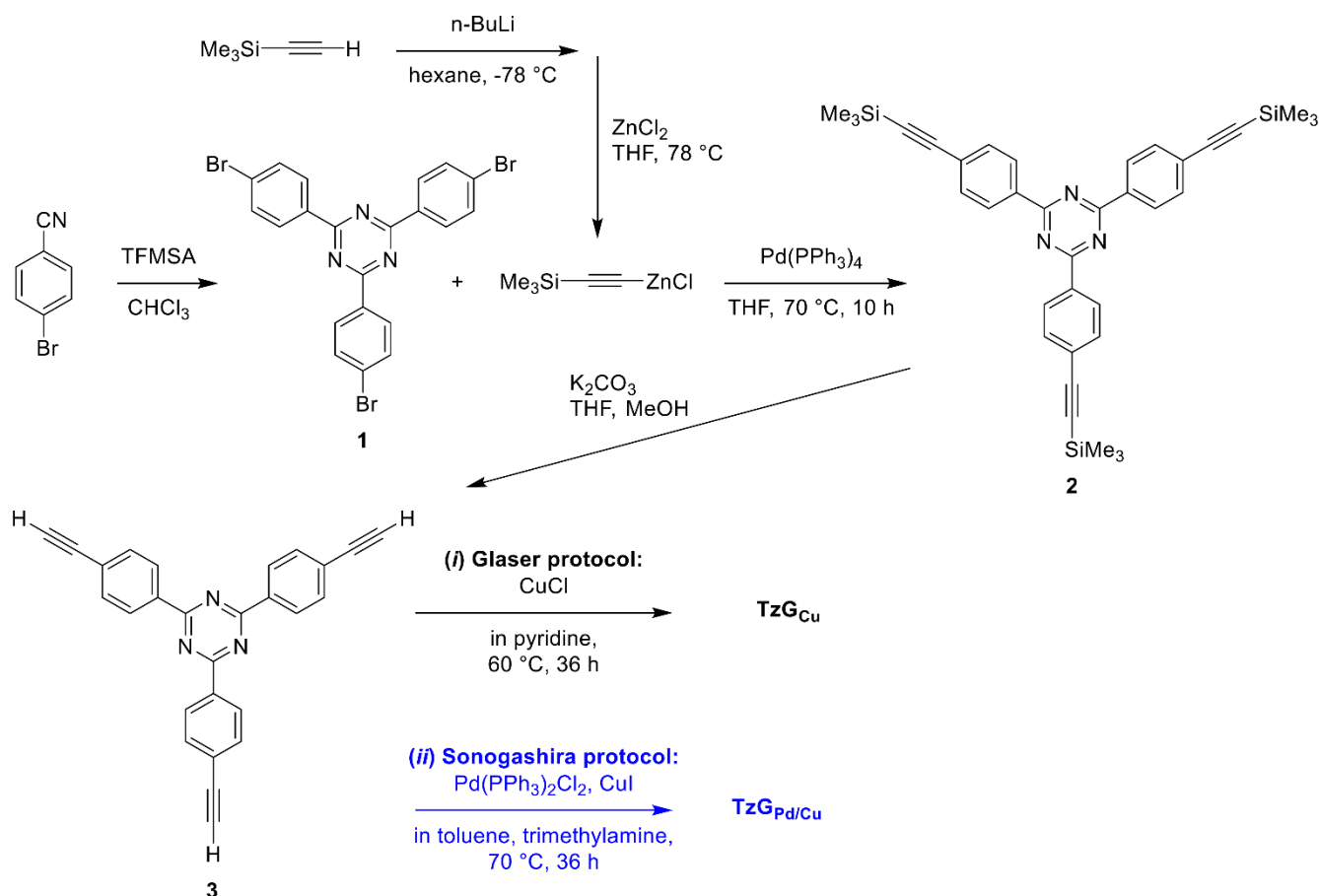
Gas sorption measurements were performed using a Micromeritics 3Flex. The Ar sorption isotherm were collected at 87 K. The surface area was calculated in the relative pressure (p/p_0) range from 0.05 to 0.35. Pore size distributions were calculated for the adsorption as well as for the desorption branch using the Barrett-Joyner-Halenda (BJH) pore model. The samples were degassed at 90 °C under vacuum before analysis.

Quantitative electron paramagnetic resonance (EPR) analysis was performed on an EMX^{plus} CW (continuous wave) EPR spectrometer (*Bruker*, Germany) equipped with the *Premium-X*-band microwave bridge. The g_{center} -factor (where $dI_{\text{EPR}}/dB = 0$) of Cu^{2+} and radical centers was determined using a built-in spectrometer frequency counter and an ER-036TM NMR-Teslameter within a standard rectangular EPR cavity, ER-4102003-ST (all *Bruker*, Germany). Quantitative EPR analysis was carried out within the ER-105000-DR double rectangular cavity using the *Bruker* "strong pitch" reference sample with known number of radicals, $3 \cdot 10^{15}$ spins / effective cm (tube length). A second identical EPR tube was used for analyzed sample. In order to provide the filling factor as closed as possible for both samples, tubes were filled and positioned within the effective EPR cavity volume in the same manner. Following experimental parameters were used for quantitative measurements: microwave frequency = 9.8176 GHz, central field = 320 mT, sweep width = 240 mT, receiver gain = $1.6 \cdot 10^4$, modulation amplitude = 0.14 mT, modulation frequency = 100 kHz, power = 3.99 mW, resolution 4801 points, conversion time = 24.0 ms and time constant = 10.2 ms. Several sweep/accumulations were applied in order to enhance the signal-to-noise ratio (S/N).

SUPPORTING INFORMATION

Synthesis

All reactions were carried out under argon atmosphere on a Schlenk line.



Scheme S1. Synthetic route towards triazine-based graphdiyne polymers.

Synthesis of 2,4,6-tris(4-bromophenyl)-1,3,5-triazine (1)

2,4,6-tris(4-bromophenyl)-1,3,5-triazine was prepared from 4-bromobenzonitrile according to the method reported by Meyer et al.^[1] ¹H NMR (400 MHz, CDCl₃): 8.61 (6H, d, J = 8.7 Hz, C₆H₄), 7.71 (6H, d, J = 8.7 Hz, C₆H₄).

Synthesis of 2,4,6-tris(4-[(trimethylsilyl)ethynyl]phenyl)-1,3,5-triazine (2)

In a 250 mL three-necked-flask 1.0 g (1.93 mmol) of 2,4,6-tris(4-bromophenyl)-1,3,5-triazine and 252 mg (0.22 mmol) Pd(PPh₃)₄ were dispersed in 40 mL anh. toluene. A solution of 10 mmol [(trimethylsilyl)ethynyl]zinc chloride in 10 mL anh. THF was prepared according to literature,^[2] and it was added drop wise to the dispersion. The mixture was stirred under argon atmosphere at 70 °C for one day. After the addition of 20 mL of 0.1 M aq. HCl, the reaction mixture was extracted with ether until the initial dark brown organic phase is transparent. The combined organic phases were washed with brine and dried over magnesium sulfate. The solvent was evaporated and further purified by chromatography on silica gel (eluent hexane/toluene = 12:1) to give 0.96 g (yield 88%) of 2,4,6-tris(4-[(trimethylsilyl)ethynyl]phenyl)-1,3,5-triazine as a white solid. ¹H NMR (400 MHz, CDCl₃): 8.68 (6H, d, J = 8.4 Hz, C₆H₄), 7.65 (6H, d, J = 8.4 Hz, C₆H₄), 0.31 (27H, s, Si(CH₃)₃).

Synthesis of 2,4,6-tris(4-ethynyl)phenyl]-1,3,5-triazine (3)

1.20 mmol 2,4,6-tris(4-[(trimethylsilyl)ethynyl]phenyl)-1,3,5-triazine was deprotected with 0.75 mmol K₂CO₃ in a THF/methanol (10:1) solution. After stirred at RT for one day, the mixture was washed with water and extracted with DCM. The combined organic phases were washed with brine and dried over MgSO₄. The solvents were evaporated to give 0.40 mg (yield 88 %).^[3] ¹H NMR (400 MHz, CDCl₃): 8.70 (6H, d, J = 8.6 Hz, C₆H₄), 7.68 (6H, d, J = 8.6 Hz, C₆H₄), 3.27 (3H, s, C≡CH).

Synthesis of triazine-based graphdiyne polymers.

(i) Glaser protocol (TzG_{Cu}). 2,4,6-tris(4-ethynyl)phenyl]-1,3,5-triazine (0.10 g, 0.25 mmol), and copper(I) chloride (25 mg, 0.25 mmol) were dissolved in 20 mL pyridine. The reaction mixture was heated to 60 °C and stirred for 36 h under argon atmosphere. Subsequently, the reaction was left to cool to RT, filtered and washed with acetone, DMF, THF, CH₃Cl, deionised water, and MeOH to remove unreacted monomer and other impurities. The polymer was cleaned up in a Soxhlet extractor using THF and MeOH for one day each. Finally, the product was dried in vacuum for 24 h at 100 °C. (Yield 98.5%; EA: cal.: C, 85.7; H, 3.17; N, 11.11, C/N = 9.0:1; found for flakes: C, 74.36; H, 3.31; N, 9.94; residue: 12.39%; C/N = 8.7:1.)

(ii) Sonogashira protocol (TzG_{Pd/Cu}). 2,4,6-tris(4-ethynyl)phenyl]-1,3,5-triazine (0.12 g, 0.32 mmol), bis-(triphenylphosphine)palladium(II) dichloride (7 mg, 3 mmol%), and copper iodide (1.8 mg, 3 mmol%) were dissolved in 4 mL toluene anhydrous and 4 mL triethylamine (Et₃N). The reaction mixture was heated to 70 °C and stirred for 36 h under argon atmosphere. Subsequently, the reaction was left to cool to RT, filtered and washed with THF, CH₃Cl, deionised water, and MeOH to remove unreacted monomer and other impurities. The polymer was cleaned up in a Soxhlet extractor using THF and MeOH for one day each. Afterwards, the product was dried in vacuum for 24 h at 100 °C. (Yield 98.2%; EA: cal.: C, 85.7; H, 3.17; N, 11.11, C/N = 9.0:1; found for flakes: C, 75.53; H, 3.99; N, 9.40; residue: 8.62%; C/N = 9.4:1.)

SUPPORTING INFORMATION

Fourier-transform infrared (FT-IR) spectroscopy

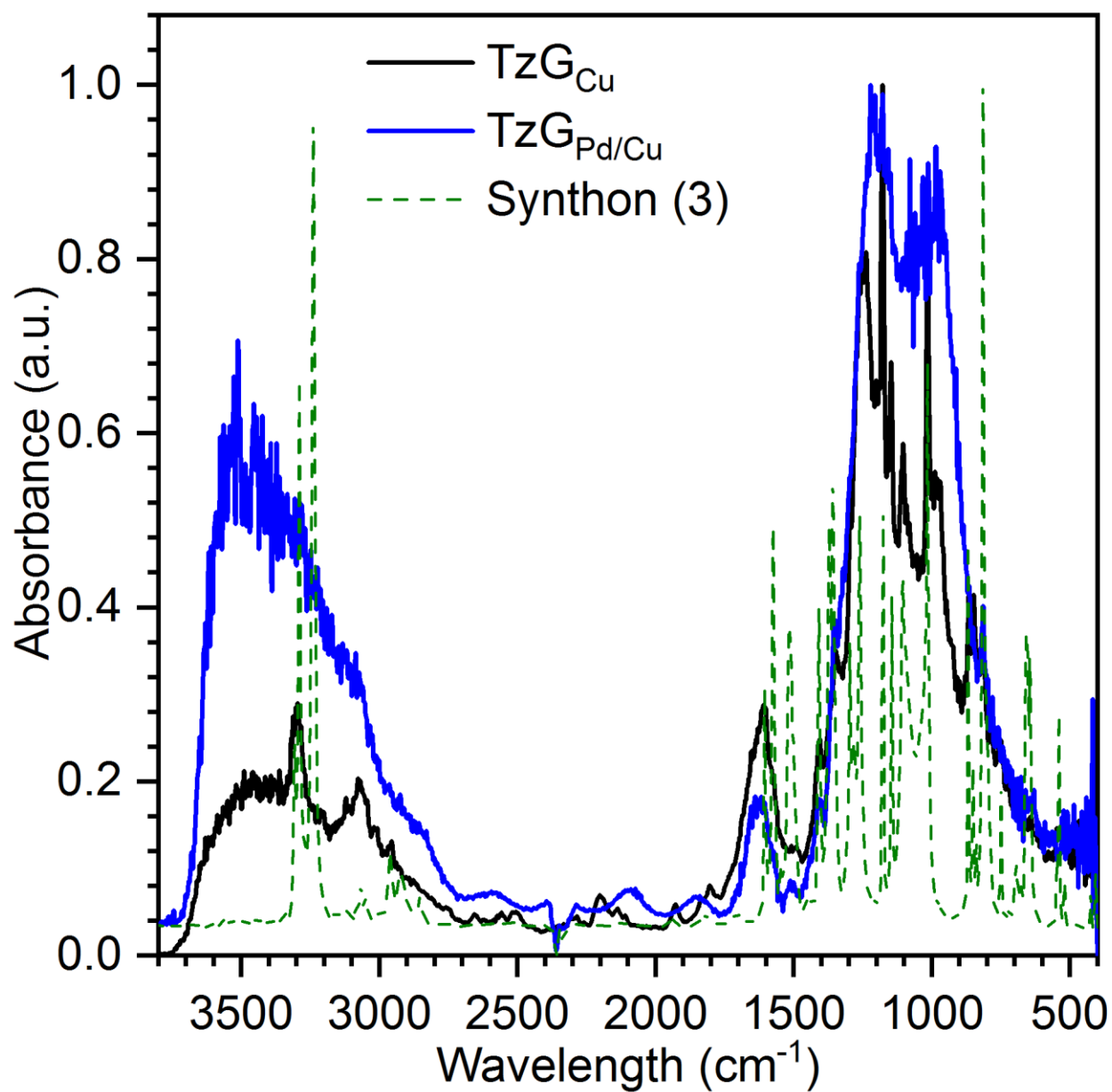


Figure S1. FT-IR spectra of TzG_{Cu} (black), TzG_{Pd/Cu} (blue), and synthon (3) (2,4,6-tris(4-ethynyl)phenyl]-1,3,5-triazine) (green).

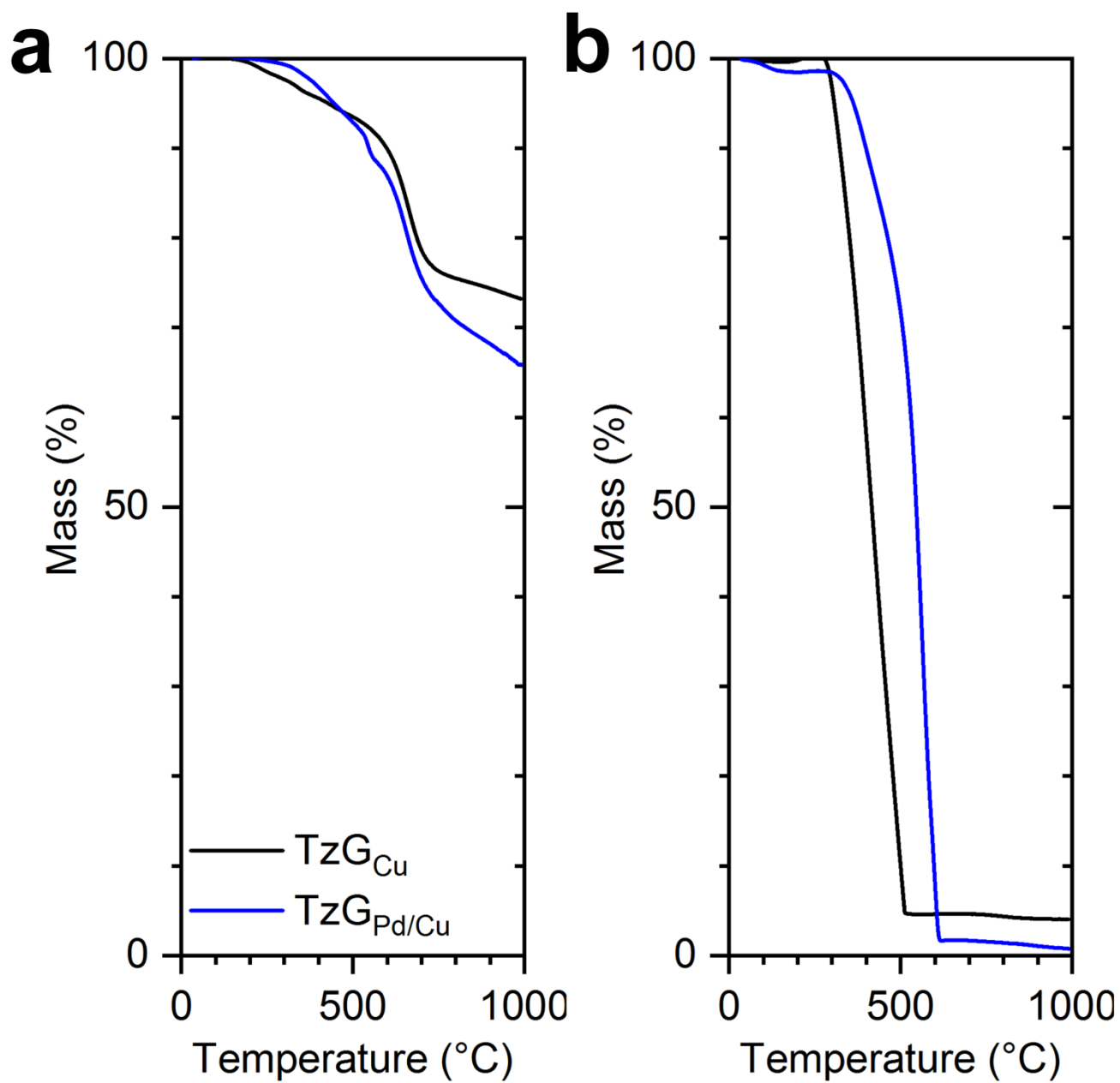


Figure S2. TGA measurements (a) under nitrogen and (b) under air of TzG_{Cu} (black), TzG_{Pd/Cu} (blue).

SUPPORTING INFORMATION

X-ray photoelectron spectroscopy (XPS)

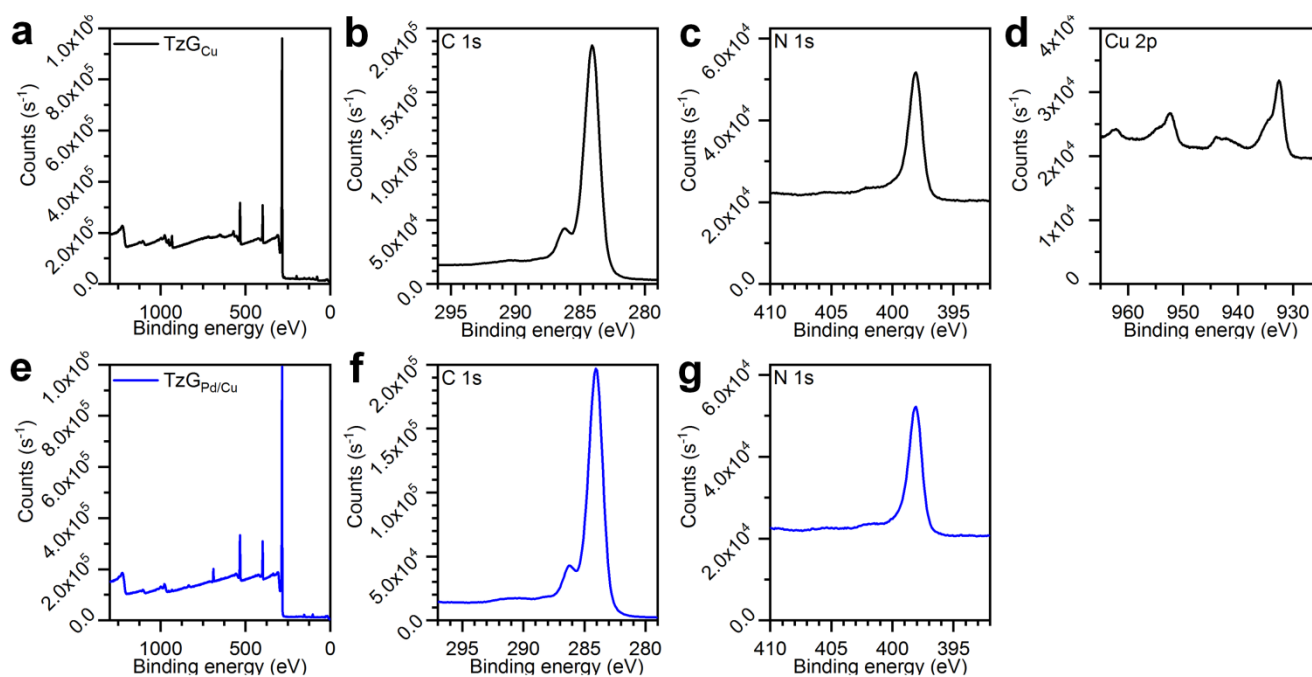


Figure S3. XPS data for of (a) TzG_{Cu} (black) and (e) TzG_{Pd/Cu} (blue) showing selected regions: (b, f) carbon 1s, (c, g) nitrogen 1s, and (d) copper 2p.

SUPPORTING INFORMATION

Energy dispersive X-ray (EDX) spectroscopy

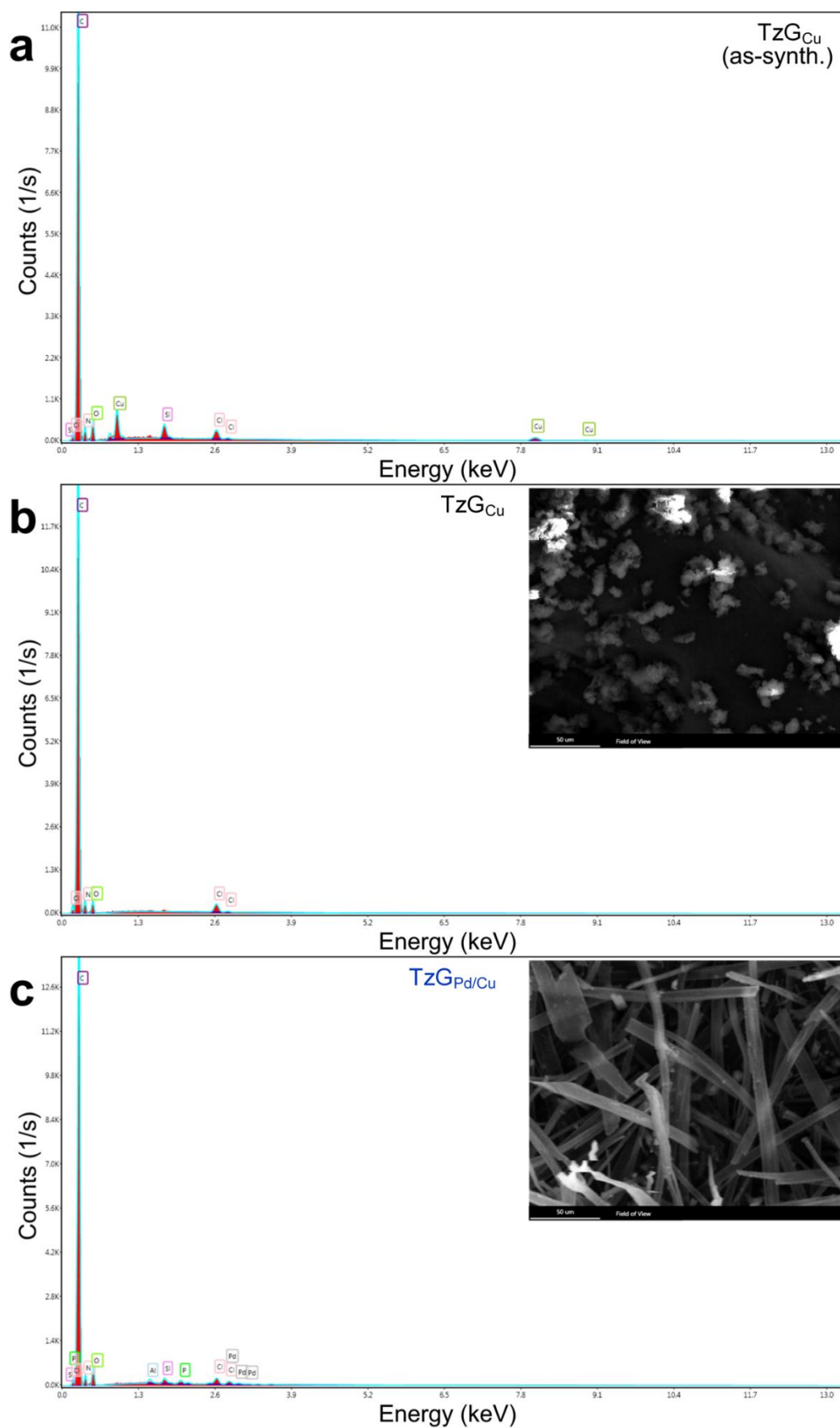


Figure S4. EDX spectra of (a) as-synthesised TzG_{Cu}, (b) TzG_{Cu} after removal of copper with FeCl₃/HCl, and (c) TzG_{Pd/Cu}. Insets in (b) and (c) show the corresponding SEM image from which EDX spectra were recorded.

SUPPORTING INFORMATION

Table S1. Ratio of elements detected by EDX, in wt%.

material	C	N	O	Cu	Cl	Pd	P
theoretical	85.7	11.11	-	-	-	-	-
TzG _{Cu}	71.51	18.02	8.09	0.85	0.61	-	-
TzG _{Pd/Cu}	69.29	17.87	11.41	0.18	0.40	0.39	0.15

Table S2. Ratio of elements detected by combustion elemental analysis (EA) and ICP-OES, in wt%.

material	C	N	H	Cu	Cl	Pd	P	I
theoretical	85.7	11.11	3.17	-	-	-	-	-
TzG _{Cu}	74.36	9.94	3.31	4.45	0.89	-	0.12	1.11
TzG _{Pd/Cu}	77.93	9.65	3.80	0.14	0.85	0.04	0.29	0.06

SUPPORTING INFORMATION

Powder X-ray diffraction (PXRD)

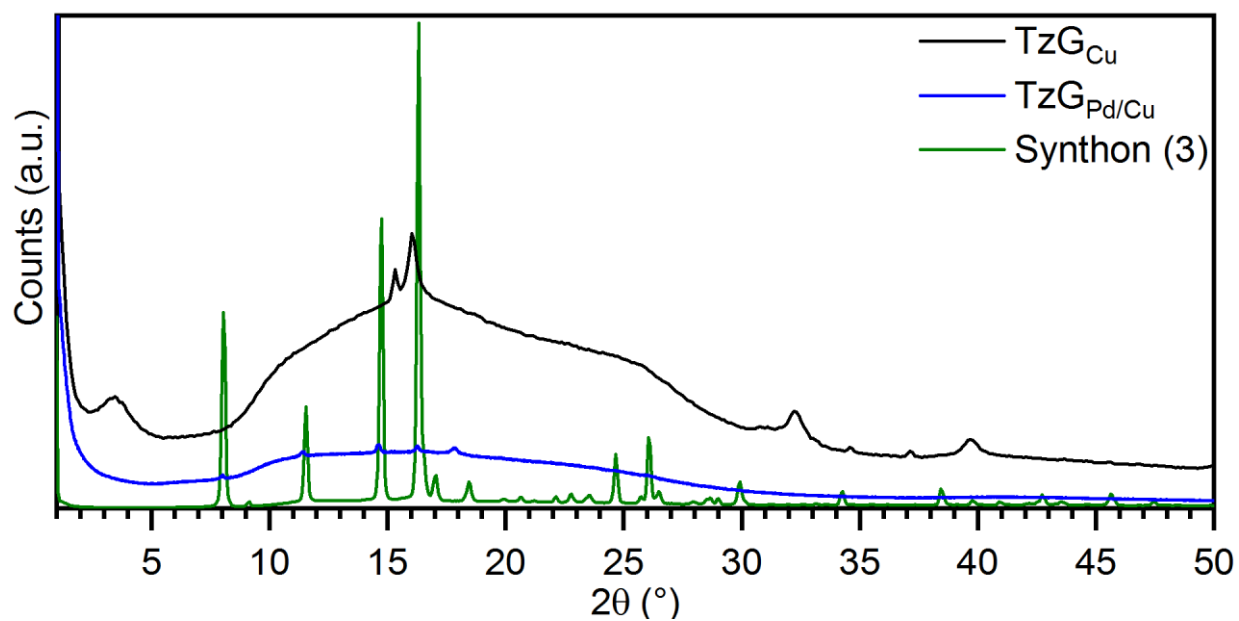


Figure S5. PXRD pattern of TzG_{Cu} (black), TzG_{Pd/Cu} (blue), and synthon (3) (2,4,6-tris(4-ethynyl)phenyl]-1,3,5-triazine) (green).

SUPPORTING INFORMATION

Transmission electron microscopy (TEM)

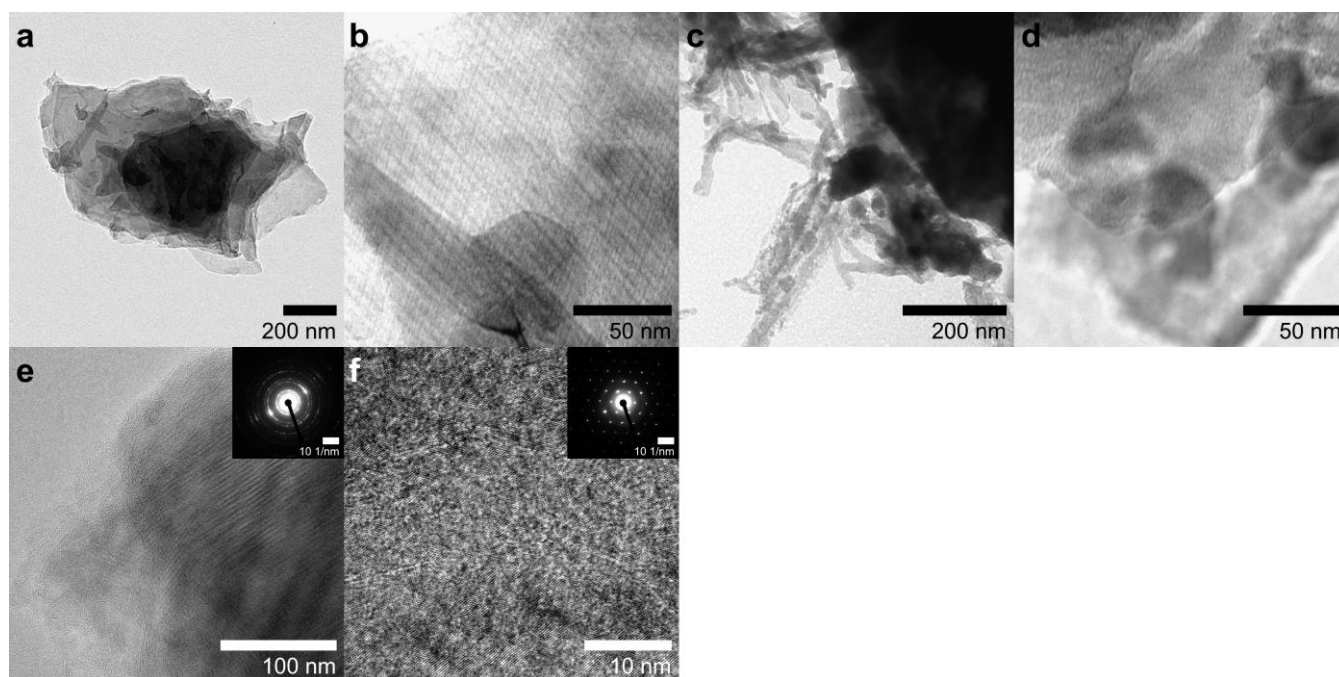


Figure S6. TEM images of (a, b) TzG_{Cu}, and (c, d) TzG_{Pd/Cu}. (e, f) TEM images of TzG_{Cu}, and the insets show the corresponding electron diffraction patterns.

Scanning electron microscopy (SEM)

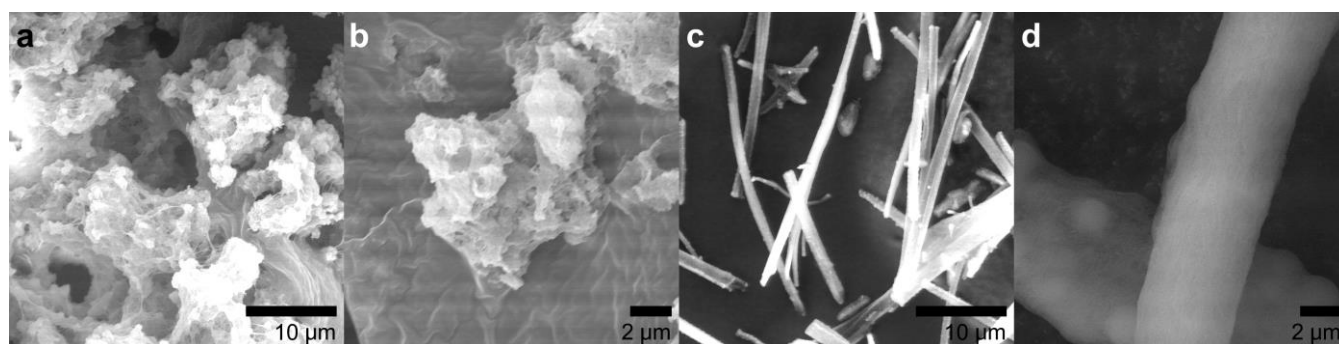


Figure S7. SEM images of (a, b) TzG_{Cu}, and (c, d) TzG_{Pd/Cu}.

SUPPORTING INFORMATION

Theoretical calculations

Two types of conceivable unit cells were obtained by various DFT methods: (1) unit cell parameters of $a = 21.5720 \text{ \AA}$, $b = 53.4858 \text{ \AA}$, $c = 5.007 \text{ \AA}$, $\beta = 95.775^\circ$, space group C2/M (no. 12), and (2) unit cell parameters of $a = b = 30.7898 \text{ \AA}$, $c = 6.1397 \text{ \AA}$, space group R-3M (no. 166). The former was considered for the rationalisation of optoelectronic and spectroscopic effects, while the latter gave the best fit in terms of crystallographic evidence (presumably due to the reduced symmetry of the hexagonal unit cell). Electron diffraction patterns were calculated on the basis of the best-candidate unit cells using CrystTBox^[4] and compared against experimentally obtained electron diffraction images.

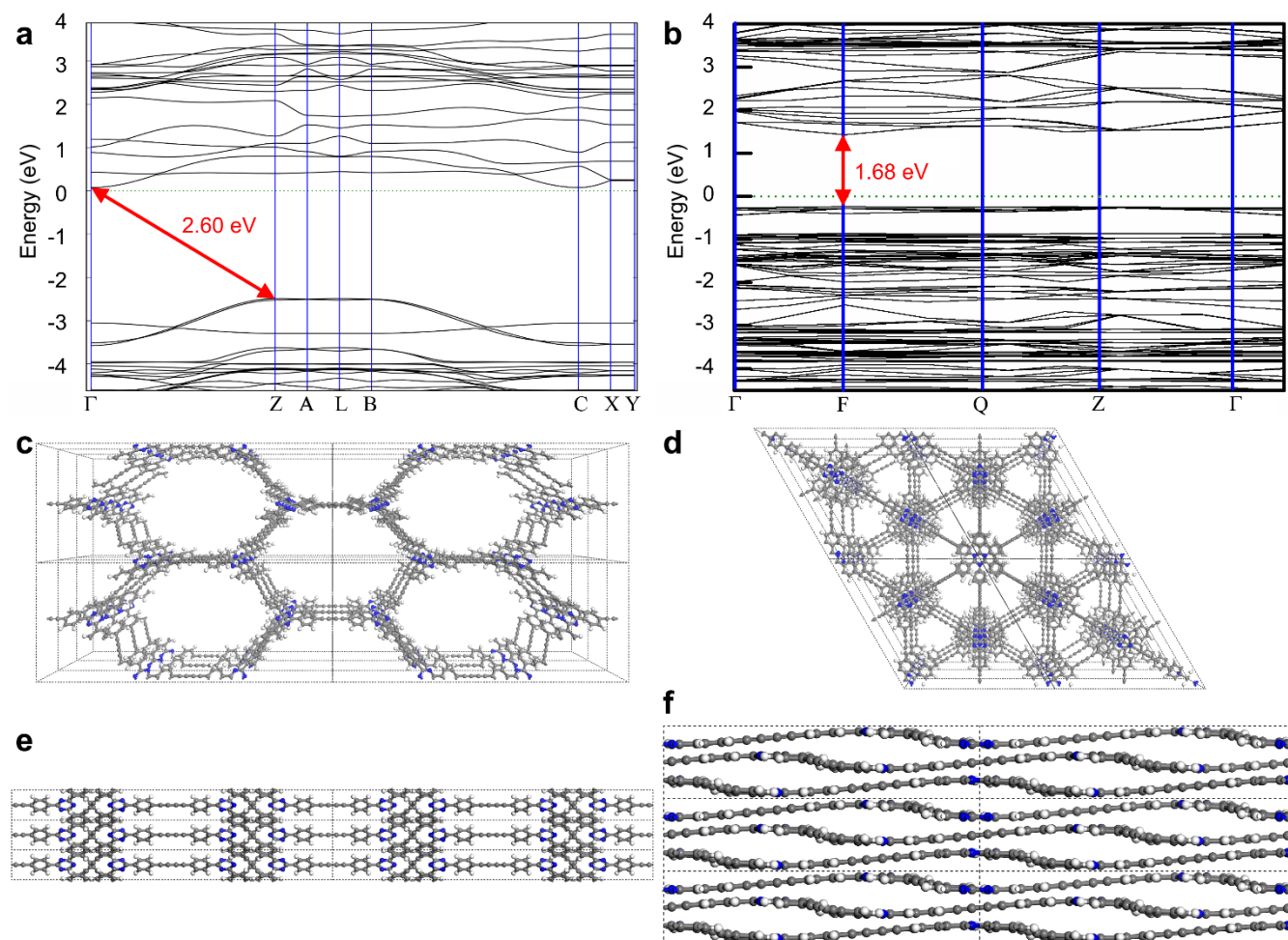


Figure S8. Band structure of TzG polymers. The Fermi level is set to zero. (a, c, e) is based on unit cell (1) with unit cell parameters of $a = 21.5720 \text{ \AA}$, $b = 53.4858 \text{ \AA}$, $c = 5.007 \text{ \AA}$, space group C2/M (no. 12), and (b, d, f) is based on unit cell (2) with unit cell parameters of $a = b = 30.7898 \text{ \AA}$, $c = 6.1397 \text{ \AA}$, space group R-3M (no. 166).

Unit cells (1) and (2) (Figure S8) were selected from a subset of conceivable structures that were obtained as follows:

Unit cell (1)

Periodic DFT calculations. First, initial structure of the triazine graphdiyne single layer periodic cell was constructed in Virtual Nano Lab (VNL) graphical environment of QuantumWise and optimised at the PBE/DZP/GD2/5x5x16k-points level using the atomistix toolkit (ATK) of QuantumWise.^[5] This yielded nicely flat layer structure (Figure S8c, e). In order to find optimal stacking of the layers we then designed ten additional periodic systems with different packing schemes using the optimized grid. Most of these structures considered layers just shifted with respect to each other. In addition, we also tried three structures with shifted and rotated grids. Each of these was then subjected to optimization with unconstrained Bravais lattice parameters at PBE/DZP/GD2/5x5x16k-points level with increased density mesh cut-off of 250 Ha. Although the enthalpy difference between the structures were of the order of $\sim 1\text{-}2 \text{ eV}$ per the unit cell only, one of the structures (Figure S8) clearly showed lowest energy/enthalpy. For this system, we then calculated the band structure, density of states etc. at the level mentioned above. The molecular structure and frontier orbital Bloch states were then visualised in VNL.

SUPPORTING INFORMATION

Quantum chemistry calculations. To further investigate the system we took the optimised unit cell structure of the grid from the periodic DFT calculations and converted it to aperiodic superstructure (or cluster model) with free valences saturated with hydrogen atoms. This seemed a reasonable choice as it contains all important features of the grid, is large enough for delocalization phenomena, yet it is still accessible to B3LYP/GD3/cc-pVTZ theory and basis set with which we have very good long term experience for organic molecules.

The molecule was then optimized at B3LYP/GD3/cc-pVTZ using Gaussian G16^[6] and molecular orbital energies were recorded. In order to confirm the applicability of the selected cluster model we also created a full ring larger grid model and performed the same set of calculations on it with a smaller basis set cc-pVDZ. The resulting HOMO-LUMO gap does not differ significantly from the one calculated on the smaller model. Therefore, we decided to proceed further on the smaller system only. In order to relate the orbital energies to water molecule level a molecule of water was also included in some of the calculations. Molden^[7] was then used to visualize the HOMO-LUMO orbitals.

Unit cell (2)

Bulk structures of the TzG material were calculated at the density functional (DFT) level, using the projector augmented-wave (PAW)^[8] formalism and a generalised gradient approximation (GGA) with the Perdew-Burke-Ernzerhof (PBE) exchange correlation function and dispersion correction (D3)^[9] as implemented in Vienna ab initio simulation package (VASP).^[10] We used a cut-off energy of 800 eV for the plane-wave basis set. The convergence criteria for energy and forces were set to 10^{-5} eV and 10^{-2} eV \AA^{-1} . The Brillouin zone (BZ) was sampled using $1 \times 1 \times 3$ gamma-centered Monkhorst-Pack grid.^[11]

Several initial structures differing mostly in the relative shift of adjacent layers were considered to find the energetically most stable, 3D bulk structure of TzG. Results are reported in Table S3. The interaction energy (E_{int}) was calculated as:

$$E_{\text{int}} = E_{\text{B}} - 2 \times E_{\text{ML}}$$

where E_{B} is the total energy of the bulk and E_{ML} is the total energy of the monolayer (calculated with the slab model using a vacuum of 15 \AA). Unit cell parameters are also reported in Table S3. The surface area and pore volume were calculated based on accessible solvent surface with the solvent radius 1.88 \AA (Ar) in Materials Studio.^[12]

Table S3. Interlayer interaction energies (E_{int}), lattice parameters (a , c , α , β , γ), unit cell volume (V) and accessible solvent surface area (S_{A}), pore volumes (V_{pore}) and densities for different TzG structures (ρ).

structure	E_{int} (kJ mol ⁻¹ per unit cell)	lattice parameters					V (\AA^3)	S_{A} (m ² g ⁻¹)	V_{pore} (cm ³ g ⁻¹)	ρ (g cm ⁻³)
		a (\AA)	c (\AA)	α ($^\circ$)	β ($^\circ$)	γ ($^\circ$)				
AA-1-serrated	-381	30.97	6.81	91	91	120	5617	2377	1.07	0.45
AA-1-inclined	-373	30.97	7.60	98	109	120	5548	2365	1.05	0.45
AA-2-serrated	-328	30.90	7.52	114	65	120	5431	2614	0.94	0.46
AA-2-inclined	-282	30.86	12.63	34	132	121	4944	3119	0.66	0.51
ABC	-336	30.81	35.75	31	149	120	3360	2102	0.13	0.75
intergrowth ^a		32.74	32.53	117	120	120	8345	7826	1.43	0.30

^a Structure investigated only at the molecular mechanics level using the UFF force field.

The SAED patterns of conceivable, calculated structures were simulated with the SingleCrystal 3 package (Figure S19).^[13] Simulations were performed for 24 layers (thicknesses of about 7.2 nm).

SUPPORTING INFORMATION

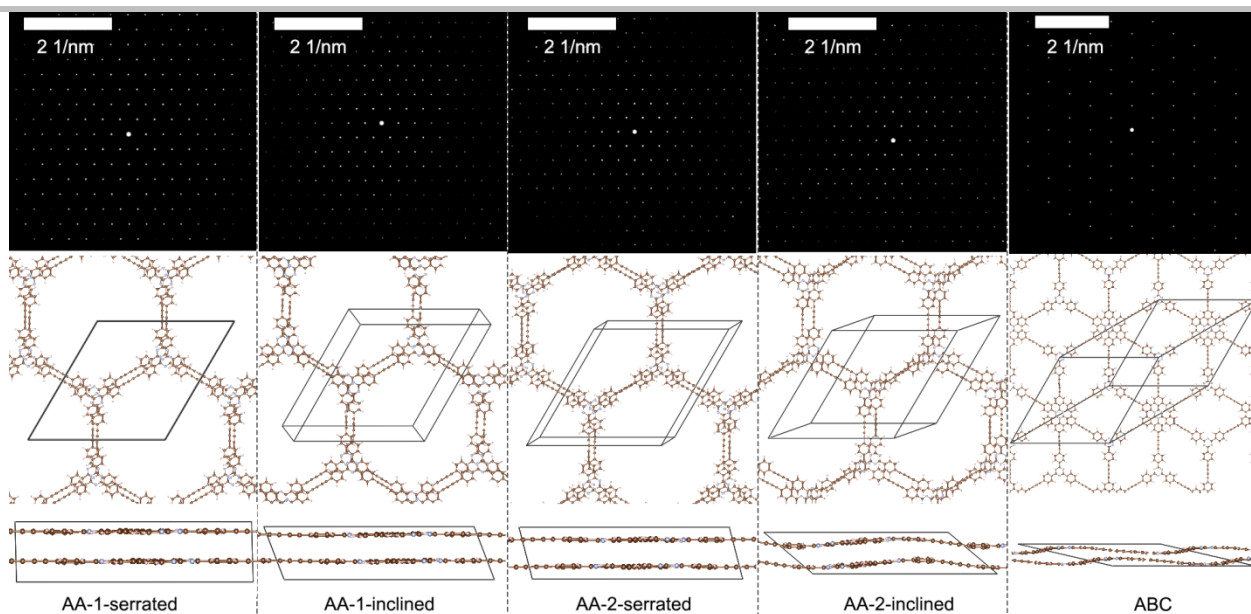


Figure S9. Band structure of TzG polymers. The Fermi level is set to zero. (a, c, g) is based on unit cell (1) with unit cell parameters of $a = 21.5720 \text{ \AA}$, $b = 53.4858 \text{ \AA}$, $c = 5.007 \text{ \AA}$, space group C2/M (no. 12), and (b, d, f) is based on unit cell (2) with unit cell parameters of $a = b = 30.7898 \text{ \AA}$, $c = 6.1397 \text{ \AA}$, space group R-3M (no. 166).

SUPPORTING INFORMATION

Argon (Ar) sorption and pore analysis

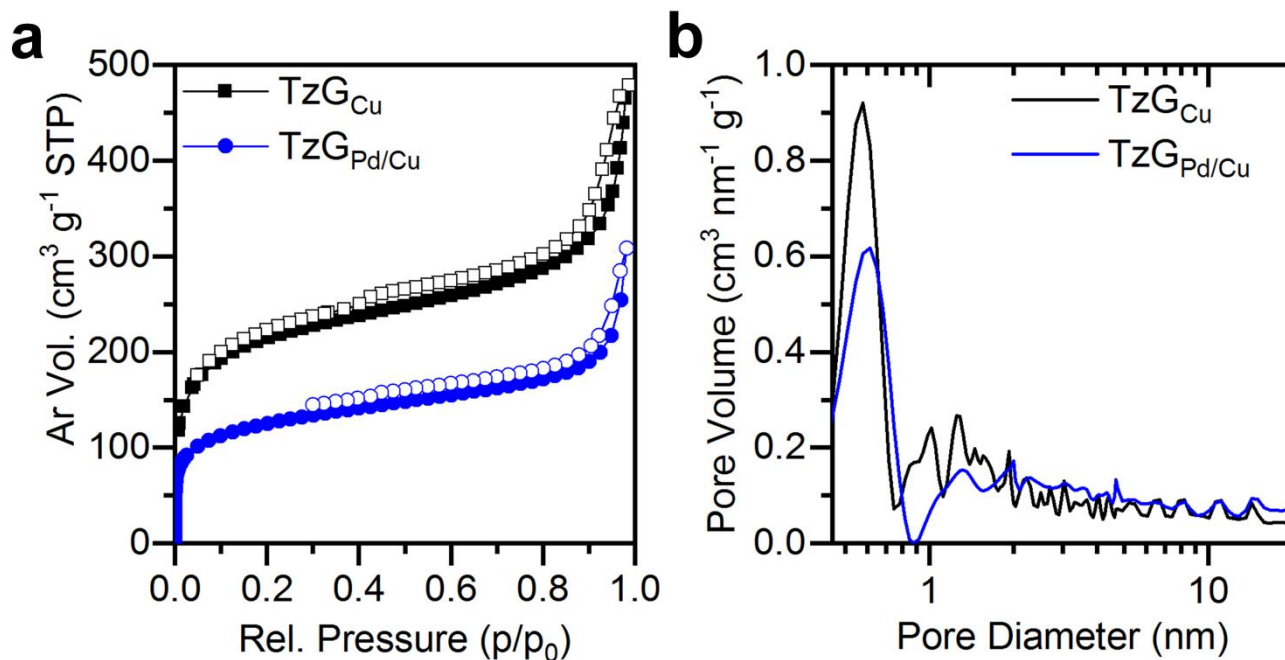


Figure S10. (a) Ar sorption isotherms for and TzG_{Cu} (black) and TzG_{Pd/Cu} (blue) measured at 88 K. (b) Pore size distribution for TzG_{Cu} (black) and TzG_{Pd/Cu} (blue) calculated with BJH for the adsorption branch of the isotherm.

Carbon dioxide (CO₂) sorption

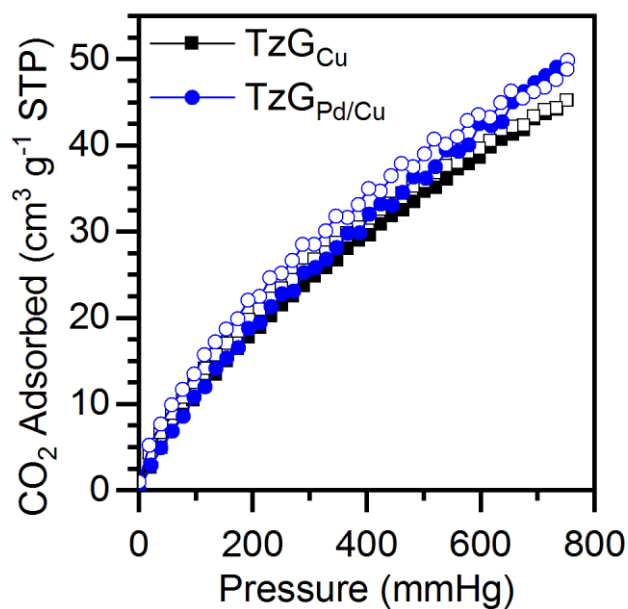


Figure S11. CO₂ sorption isotherms for and TzG_{Cu} (black) and TzG_{Pd/Cu} (blue) measured at 273 K.

SUPPORTING INFORMATION

Porosity parameters

Table S4. Porosity parameters of TzG polymorphs.

Sample	S_{BET} ($\text{m}^2 \text{g}^{-1}$) ^[a]	V_{tot} ($\text{cm}^3 \text{g}^{-1}$) ^[b]	V_{micro} ($\text{cm}^3 \text{g}^{-1}$) ^[c]	CO_2 uptake (mmol g^{-1}) ^[d]
TzG _{Cu}	660	0.53	0.12	2.02
TzG _{Pd/Cu}	392	0.32	0.07	2.23

[a] Surface area calculated from the adsorption branch of the Ar isotherm using the BET equation (S_{BET}). [b] Total pore volume (V_{tot}) calculated from Ar uptake at $p/p_0 = 0.95$. [c] Micro pore volume (V_{micro}) calculated from Ar uptake at $p/p_0 = 0.10$. [d] CO_2 uptake calculated at 273 K and 1 bar.

Photocatalysis

Photocatalytic hydrogen evolution experiments were carried out in a jacketed 3-neck quartz reactor with a total volume of 36 mL (Figure S15). 10 mg of catalyst was dispersed in 18 mL water:acetonitrile mixture (1:1) and 2 mL TEOA. The reactor was closed using rubber septa, completely evacuated and purged with argon to remove any air and then irradiated with a 300 W Xe lamp (L.O.T.-Quantum design) equipped with a cut off filter of 395 nm. Headspace volume was calculated to be 16 mL.

Control experiments “in the dark” were performed to verify that no hydrogen is being evolved prior to illumination. During catalytic reactions, the temperature was kept fixed at 20 °C using a thermostat. Distance between the reactor and light source was also kept fixed at 10 cm and stirring speed was maintained at 600 rpm. Gas samples from the head space were taken after 15 h of reaction and were analyzed by GC equipped with a TCD detector.



Figure S13. Photos of the reactor (left) catalytic reaction setup (right).

Author Contributions

D.S. conceived and designed the experiments, performed the synthetic experiments, analysed the data, and wrote the paper. A.A. performed photocatalytic tests and analysed the data. A.I. and M.J.B. performed the high-resolution transmission electron microscopy (HR-TEM) and analysed the data. Y.S.K. performed TGA and photoluminescence measurements and analysed the data. M.V.O. and J.C. performed Ar sorption tests and analysed the data. J.T. performed the electron paramagnetic resonance (EPR) tests, and analysed the data. J.S. performed X-ray photoelectron spectroscopy (XPS) experiments and analysed the data. J.V.C., J.V., P.L., and P.N. performed DFT calculations and analysed the data. J.C., P.N., A.T., and M.J.B. contributed reagents/materials/analysis tools. M.J.B. conceived and designed the experiments, analysed the data, and wrote the paper.

References

- [1] A. Ranganathan, B. C. Heisen, I. Dix, F. Meyer, *Chem. Commun.* **2007**, 3637-3639.
- [2] A. O. King, E. Negishi, F. J. Villani, A. Silveira, *J. Org. Chem.* **1978**, *43*, 358-360.
- [3] Z. Jing, *J. Chem. Pharm. Res.* **2014**, *6*, 322-326.
- [4] a) M. Klinger, *J. Appl. Crystallogr.* **2017**, *50*; b) M. Klinger, A. Jäger, *J. Appl. Crystallogr.* **2015**, *48*; c) M. Klinger, Institute of Physics of the Czech Academy of Sciences, **2015**.
- [5] a) J. M. Soler, E. Artacho, J. D. Gale, A. Garcia, J. Junquera, P. Ordejon, D. Sanchez-Portal, *J. Phys. Condens. Matter* **2002**, *14*, 2745-2779; b) M. Brandbyge, J. L. Mozos, P. Ordejon, J. Taylor, K. Stokbro, *Phys. Rev. B* **2002**, *65*; c) G. W. T. M. J. Frisch, H. B. Schlegel, G. E. Scuseria, M. A. Robb, J. R. Cheeseman, G. Scalmani, V. Barone, G., A. Petersson, H. Nakatsuji, X. Li, M. Caricato, A. V. Marenich, J. Bloino, B. G. Janesko, R. Gomperts, B. Mennucci, H. P. Hratchian, J. V. Ortiz, A. F. Izmaylov, J. L. Sonnenberg, D. Williams-Young, F. Ding, F. Lipparini, F. Egidi, J. Goings, B. Peng, A. Petrone, T. Henderson, D. Ranasinghe, V. G. Zakrzewski, J. Gao, N. Rega, G. Zheng, W. Liang, M. Hada, M. Ehara, K. Toyota, R. Fukuda, J. Hasegawa, M. Ishida, T. Nakajima, Y. Honda, O. Kitao, H. Nakai, T. Vreven, K. Throssell, J. A. Montgomery, Jr., J. E. Peralta, F. Ogliaro, M. J. Bearpark, J. J. Heyd, E. N. Brothers, K. N. Kudin, V. N. Staroverov, T. A. Keith, R. Kobayashi, J. Normand, K. Raghavachari, A. P. Rendell, J. C. Burant, S. S. Iyengar, J. Tomasi, M. Cossi, J. M. Millam, M. Klene, C. Adamo, R. Cammi, J. W. Ochterski, R. L. Martin, K. Morokuma, O. Farkas, J. B. Foresman, and D. J. Fox, *Gaussian*, **2016**.
- [7] G. Schaftenaar, J. H. Noordik, *J. Comput.-Aided Mol.* **2000**, *14*, 123-134.
- [8] J. P. Perdew, K. Burke, M. Ernzerhof, *Phys. Rev. Lett.* **1996**, *77*, 3865-3868.
- [9] S. Grimme, J. Antony, S. Ehrlich, H. Krieg, *J. Chem. Phys.* **2010**, *132*, 19.
- [10] a) G. Kresse, J. Hafner, *Phys. Rev. B* **1993**, *47*, 558-561; b) G. Kresse, D. Joubert, *Phys. Rev. B* **1999**, *59*, 1758-1775.
- [11] H. J. Monkhorst, J. D. Pack, *Phys. Rev. B* **1976**, *13*, 5188-5192.
- [12] D. S. BIOVIA, Materials Studio v7.0 ed., San Diego: Dassault Systèmes, **2013**.
- [13] C. S. Limited, SingleCrystal™ ed., CrystalMaker Software Ltd, Oxford, UK, **2017**.